Apolipoprotein A-I configuration and cell cholesterol efflux activity of discoidal lipoproteins depend on the reconstitution process.

Luz Ángela Cuellar[1], Eduardo Daniel Prieto[1], Laura Virginia Cabaleiro and Horacio Alberto Garda

Instituto de Investigaciones Bioquímicas de La Plata (INIBIOLP). Consejo Nacional de Investigaciones Científicas y Técnicas (CONICET)/ Universidad Nacional de La Plata (UNLP). Facultad de Ciencias Médicas. Calles 60 y 120. 1900 - La Plata, Argentina.

[1]These authors made an equal contribution to this work.

Corresponding author: Horacio A. Garda, Instituto de Investigaciones Bioquímicas de La Plata (INIBIOLP). Facultad de Ciencias Médicas. Calles 60 y 120. 1900 - La Plata, Argentina; Tel: +54 221 482 4894; Fax: +54 221 425 8988; Email: hgarda@med.unlp.edu.ar.

ABSTRACT

Discoidal high-density lipoproteins (D-HDL) are critical intermediates in reverse cholesterol transport. Most of the present knowledge of D-HDL is based on studies with reconstituted lipoprotein complexes of apolipoprotein A-I (apoA-I) obtained by cholate dialysis (CD). D-HDL can also be generated by the direct microsolubilization (DM) of phospholipid vesicles at the gel/fluid phase transition temperature, a process mechanistically similar to the "in vivo" apoAI lipidation via ABCA1. We compared the apoA-I configuration in D-HDL reconstituted with dimyristoylphosphatidylcholine by both procedures using fluorescence resonance energy transfer measurements with apoA-I tryptophan mutants and fluorescently labeled cysteine mutants. Results indicate that apoA-I configuration in D-HDL depends on the reconstitution process and are consistent with a "double belt" molecular arrangement with different helix registry. As reported by others, a configuration with juxtaposition of helices 5 of each apoAI monomer (5/5 registry) predominates in D-HDL obtained by CD. However, a configuration with helix 5 of one monomer juxtaposed with helix 2 of the other (5/2 registry) would predominate in D-HDL generated by DM. Moreover, we also show that the kinetics of cholesterol efflux from macrophage cultures depends on the reconstitution process, suggesting that apoAI configuration is important for this HDL function.

Keywords: Apolipoproteins, Fluorescence resonance energy transfer (FRET), Lipoprotein structure, Site directed mutagenesis, Single tryptophan mutants, Cysteine mutants.

Footnotes:

[1]These authors made an equal contribution to this work.

[2]Abbreviations: ABCA1, ATP binding cassette A1; ABCG1, ATP binding cassette G1; apoA-I, apolipoprotein A-I; CD, cholate-dialysis; D-HDL, discoidal high density lipoproteins; DM, direct microsolubilization; DMPC, 1,2-dimyristoyl phosphatidyl choline; DPPC, 1,2-dipalmitoyl phosphatidyl choline; FRET, fluorescence resonance energy transfer; GdnHCl, guanidine hydrochloride; HDL, high density lipoproteins; IPTG, isopropyl-1-thio-β-D-galactopyranoside; LCAT, lecithin-cholesterol acyl transferase; MLV, multilamellar vesicles; PAGE, polyacrylamide gel electrophoresis; PAGGE, polyacrylamide gradient gel electrophoresis; POPC, 1-palmitoyl, 2-oleoyl phosphatidyl choline; RCT, reverse cholesterol transport; SR-BI, scavenger receptor BI; Tt, gel to liquid-crystalline phase transition temperature.

1. INTRODUCTION

Apolipoprotein A-I[2] (apoA-I), the major protein of high-density lipoproteins (HDL), plays a key role in reverse cholesterol transport (RCT), a process with high antiatherogenic relevance that delivers cholesterol excess from tissues toward the liver for catabolism and elimination [1]. Lipid-free or lipid-poor apoAI is initially lipidated at the cell membrane in a process depending on the cholesterol/phospholipid transfer activity of ATP binding cassette A1 (ABCA1) whose deficiency causes a severe HDL deficiency syndrome known as Tangier's disease [2]. As proposed by Vedhachalam et al. [3], phospholipid translocation from the inner toward the outer membrane leaflet via ABCA1 induces bending of the membrane bilayer to create high curvature sites to which apoA-I can bind and microsolubilize membrane lipids to generate nascent discoidal HDL (D-HDL) particles. Nascent D-HDL particles created in this way contain some cholesterol [4], but they are able to acquire additional cholesterol by several mechanisms mediated or not by cellular proteins. Among protein-mediated mechanisms, we can mention the active transport catalyzed by ABCG1, another member of the ABC transporter family [5], and the facilitated transport via the scavenger receptor BI (SR-BI) [6]. Mechanisms independent of cell membrane proteins include the so-called aqueous diffusion pathway [7] involving desorption of cholesterol molecules from cell membrane, followed by their diffusion in the aqueous phase and collision-mediated absorption into HDL particles [8]. Besides, it was also proposed [9,10] that membrane cholesterol desorption and transference to D-HDL can be facilitated by the membrane anchoring of D-HDL particles through the insertion into the lipid bilayer of the central apoA-I 3-4 helix-pair.

Once enriched in cholesterol, D-HDL are good substrates of lecithin-cholesterol acyl transferase (LCAT) that generates a hydrophobic core of cholesteryl ester converting the discs into the spherical HDL commonly found in plasma [11]. Spherical HDL are remodeled in circulation by several processes as lipid or apolipoprotein exchange with other circulating lipoproteins, lipolysis, and liver selective cholesteryl ester uptake by SR-BI [1]. Most of these processes result in release of free or lipid-poor apoA-I able to be relipidated by the ABCA1 reaction.

Thus, D-HDL are very important intermediates in apoA-I mediated cell cholesterol efflux. Detailed knowledge of apoA-I structure in D-HDL is important for understanding the molecular life cycle of HDL. Being short-lived, D-HDL are not easily isolated from plasma, and most of the knowledge on their structure and properties was obtained with artificially reconstituted complexes. The most used procedure to reconstitute D-HDL is the cholate dialysis (CD) method developed by Matz and Jonas [12]. It consists in the preparation of mixed micellar dispersion of apoA-I, lipids and cholate; and ulterior removal of cholate by dialysis. Alternatively, D-HDL can be generated by direct microsolubilization (DM) of phospholipid vesicles at the gel to liquid-crystalline phase transition temperature (Tt). The DM method can be mechanistically similar to the "in vivo" D-HDL generation mediated by ABCA1 at the cell membrane [13], but it is restricted only to those phospholipids suffering the phase transition at compatible temperatures as dipalmitoyl- (DPPC, Tt = 41°C) or dimyristoyl- (DMPC, Tt = 24°C) phosphatidylcholines. The CD method, on the contrary, can be used with any phospholipid including those physiological ones which have unsaturated fatty acids as palmitoyl-oleyl-phosphatidylcholine (POPC), that suffer the phase transition at subzero temperatures.

Both approaches generate differently sized D-HDL particles which contain 2, 3 or more apoA-I molecules. The best characterized ones have a hydrated diameter of 9.6 nm. These particles contain two molecules of apoA-I with about 100-150 phospholipid molecules. Several models have been proposed for D-DHL [14,15], but the one with the best theoretical and experimental support is the "double belt" model in which each of two ring-shaped apoA-I molecules wraps around a patch of phospholipid bilayer in an antiparallel orientation, each one on its own leaflet, and with the long helical axis perpendicular to the acyl chains [16-20]. The crystal structure of apoAI Δ1-43 [21], in spite of lacking lipid, shows apoA-I in a ring-shaped oligomer implying that apoA-I may prefer a belt-like orientation in lipoproteins. A similar belt-like orientation seems to be adopted by other exchangeable apolipoproteins in particles of similar discoidal morphology [22-25].

Another question to be analyzed is the spatial relationship between both apoAI molecules on the disc. Computer analysis [17] predicted a registry between the monomers with similar intermolecular salt bridge connections as in apoAI Δ1-43 [21] crystal structure. In this model [17], helix 5 of each apoA-I molecule lies in direct opposition (5/5 orientation, see figure 1). Juxtaposition of helices 5 is also observed in a recently obtained crystal structure of the C-terminal truncated form Δ(185-243) apoAI [26]. The question was addressed by the group of WS Davidson in discoidal [27] and spherical HDL [28] reconstituted particles as well as in HDL isolated from human plasma [29] using lysine cross-linking followed by trypsinolysis and mass spectrometry analysis of the resulting peptides. In D-HDL reconstituted with POPC through the CD method [27], they found several intermolecular distance constraints supporting the double-belt model with the 5/5 registry, but data also indicate the presence of an additional double-belt orientation with a shifted helical registry with juxtaposition between helices 5 and 2 (5/2 registry) (see figure 1). Interestingly, the cross-linking pattern found in reconstituted spherical HDL was highly similar to that found in discs, regardless of whether they contained two or three molecules of apoA-I in each particle [28]. Moreover, the same methodology applied to 5 HDL subfractions isolated from human plasma revealed the presence of several crosslinks supporting the double belt 5/5 or 5/2 arrangement [29]. Bath et al. [30] used a very similar approach with CD reconstituted D-HDL to find three intermolecular cross-links, two of which were consistent with the 5/5 double-belt model. The third crosslink (K12-K182) was interpreted as indicative of a hairpin centered around residue 44 in such a way that the N terminus interacts with the C-terminal portion of the second apoA-I molecule that has also doubled back on itself. As noted by Davidson and Thompson [31], however, this cross-link is also quite consistent with the shifted 5/2 double belt proposed by Silva et al. [27]. Recently, Sorci-Thomas et al. [32] studied the structure of two kinds of nascent HDL generated by the action of ABCA1 of human embryonic kidney cells. Both in 7.5 and 10 nm particles containing respectively 2 and 3 apoAI molecules, they found several intermolecular lysine cross-links indicative of the 5/5 double-belt configuration besides a cross-link in each kind of particle (K182-K239 and K94-K96) that does not fit this arrangement. These cross-links were interpreted as indicative of a hairpin in 7.5 nm particles and a triple belt in 10 nm HDL. However, both cross-links can be alternatively interpreted as fitting the 5/2 registry. Irrespective of how these crosslinks are interpreted, all these studies indicate that the basic belt configuration of apoAI is maintained in HDL particles of different size, shape and origin.

Concerning this work, we were interested in determining whether apoAI configuration on discs depends on the reconstitution method. With this aim, we have used two single tryptophan mutants and three cysteine mutants specifically designed to distinguish between the 5/5 and 5/2 orientations. Intermolecular distances (or distances constraints) obtained from self-quenching and fluorescence resonance energy tranfer (FRET) between identical (homo-FRET) or different (hetero.FRET) fluorophores strongly indicated that apoAI configuration in D-HDL prepared by DM of DMPC vesicles at Tt (24°C) is different from that of D-HDL prepared with the same lipid by CD. Data are consistent with the predominance of the 5/5 orientation in CD prepared D-HDL, and the 5/2 configuration in D-HDL prepared by DM. Besides, cholesterol efflux measurement from murine macrophages showed a different behaviour between both D-HDL preparations, indicating that helix registry would be relevant for D-HDL function.

2. MATERAL AND METHODS

2.1 Serum apoAI.

It was obtained as previously described [33] from human serum kindly donated by Banco de Sangre, Instituto de Hemoterapia de la Provincia de Buenos Aires, La Plata, Argentina. It showed more than 95% purity as estimated by SDS–polycrylamide gel electrophoresis (SDS–PAGE).

2.2 ApoAI single tryptophan and cysteine mutants.

The cDNA constructions of single tryptophan mutants W@104 and W@108 as well as the procedures for their expression and purification were described in a previous report [34].

For obtaining the cysteine mutants (K107C, K133C and K226C) we started from the cDNA of human pro-apoAI kindly donated by Dr A. Jonas (University of Illinois at Urbana-Champaign, IL, USA) inserted into a pET-30 plasmid (Novagen, Madison, WI, USA), which was modified in our laboratory [35] in order to create an acid labile Asp-Pro peptide bond between amino acids 2 and 3 allowing the specific chemical cleavage of the N-terminal region containing the pro-segment and the His-Tag fusion peptide [36]. This construction was employed as template to introduce the corresponding mutations for K107C, K133C and K226C using the QuickChange site directed mutagenesis kit (Stratagene, La Jolla, CA, USA). Primers were designed according to the instructions of kit manufacturers and their sequences are given in Supplemental Data (table S-I). PCR reactions were performed using *Pfu*DNA polymerase. After template digestion with Dpn1, competent cells were transformed with PCR products, and the plasmid DNAs of transformed bacteria were sequenced from S-tag and T7-terminator sites. The service of Macrogen Inc. (Seoul, Korea) was used for primer synthesis and DNA sequencing.

BL21 (DE3) expression host cells were transformed with plasmids containing the correct sequences. After induction with isopropyl-1-thio-β-D-galactopyranoside (IPTG), the His-tagged fusion proteins were extracted with 3 M guanidine hydrochloride (GdnHCl) and purified by immobilized metal affinity chromatography on Ni columns (GE Healthcare Bio-Sciences AB, Uppsala, Sweden) using 0.5 M imidazole for their elution. Fusion proteins were cleaved by 45 % formic acid at 45 °C for 5 h [36]. Then, proteins were taken to pH 7.4 in 3 M GdnHCl and exhaustively dialyzed against phosphate buffer. A second metal affinity chromatography step, where the cysteine mutants were eluted with 0.05 M imidazole, was used for separating the final proteins from contaminants His-tag and rests of non cleaved fusion protein. SDS-polyacrylamide gel electrophoresis (PAGE) was used for checking each step during expression and purification. The final yield was 5 to 8 mg of protein per liter of culture medium and purity was higher than 95% as judged by SDS-PAGE. Proteins were stored in 3.0 M GdnHCl at -80°C.

2.3 Characterization of apoAI mutants.

W@104 and W@108 mutants were previously characterized [34]. Their far UV circular dichroism spectra were similar to that of serum apoAI. Although they showed a lower rate of DMPC vesicle microsolubilization at 24°C, the maximal clearing efficiency was similar to that of serum apoAI [34].

Cysteine mutants and wild type apoAI used in the present work lack the first two residues at their N terminal, which are lost after the acidic cleavage to eliminate the His-tag. However, neither the folding properties nor the ability to solubilize vesicles is affected by this change [35].

The possible influence of K107C, K133C and K226 mutations on apoAI folding and structure was herein discarded by using different fluorescence approaches (see table S-II in Supplemental Data). Tryptophan fluorescence emission and denaturation curves at increasing concentrations of GdnHCl were indistinguishable among cysteine mutants and the wild type protein. Besides, no difference was found in the efficiency for acrylamide quenching, bis-ANS binding or tryptophan to bis-ANS FRET efficiency. Also, substitutions of lysine 107, 133 or 226 by cysteine did not evoke any difference in the rate of DMPC clearance at 24°C (not shown).

2.4 Labeling of cysteine mutants.

Mutants were labeled with C5 maleimide derivatives of Alexa Fluor-350, -488 and -647 from Molecular Probes, Eugene, OR. Proteins at a concentration of 40 μM in 3.0 M GdnHCl were incubated with 10-fold molar excess of tris(2-carboxyethyl)phosphine hydrochloride (TCEP) for 1 h to reduce the -SH group. A 10 mM stock solution of dyes in dimethyl sulfoxide was added so that the final molar ratio of probe to protein was 5:1. Reaction mixtures were then incubated at room temperature in the darkness for 3 h, and 0.4 mM glutathione was added to stop the reaction. Excess of dye was removed by ultrafiltration with Centricon filters with 10 kDa cut-off membranes (Millipore). Samples (2.0 ml) were concentrated to 0.1-0.15 ml by spinning at 5000xg. Concentrates were diluted to the original volume with 3.0 M GdnHCl and procedure was repeated 3 times.

Absorption spectra were measured in an Agilent 8453 Diode Array Spectrophotometer. The degree of labeling was determined by calculating the dye concentrations from their optical densities at the

corresponding absorption maxima using the extinction coefficients of 1.9 10^4, 7.2 10^4, and 2.6 10^5 M^{-1} cm^{-1} for Alexa-350, Alexa-488 and Alexa-647, respectively. Protein concentration was estimated from the second-derivative spectra corresponding to tryptophan absorption using unlabeled wild type apoAI of known concentration as standard, and by using the Protein Assay Kit for Qubit fluorometer (Invitrogen). The calculated labeled efficiency was within the range of 0.9 and 1.1 for all samples. Identical labeling and dye removal conditions used with wild type apoAI indicated that non-specific labeling was lower than 3 %.

No spectral shift in tryptophan fluorescence emission of the labeled proteins was detected, indicating that labeling did not affect either folding or conformation (not shown).

2.5 Reconstitution of D-HDL.

Dimyristoyl phosphatidylcholine (DMPC) in chloroform was dried down by flushing N2 in a glass tube leaving a thin lipid layer. Lipids were brought up in 25 mM sodium phosphate buffer to a lipid concentration of 10 mM. Multilamellar vesicles (MLV) were made by extensive vortexing at 35°C. Proteins (or protein mixtures) in 3.0 M Gdn HCl were dialyzed against 25 mM sodium phosphate buffer pH 7.4 immediately before use.

For D-HDL reconstitution by CD, the method of Matz and Jonas [12,37] was used. Proteins (or protein mixtures) were mixed with DMPC-MLV and sodium cholate in a 1/40/60 molar ratio and then dialyzed exhaustively against 25 mM sodium phosphate buffer pH 7.4. For reconstitution by direct microsolubilization (DM D-HDL), DMPC-MLV were incubated with proteins (or protein mixtures) at the DMPC phase transition temperature (24°C) at a 40/1 lipid/protein molar ratio for 24 h. The decrease in turbidity with time was analyzed by following the Optical Density at 350 nm. A similar rate of MLV microsolubilization was observed for the differently labeled proteins. In both cases (CD and DM D-HDL), samples were subjected to 5 cycles of temperature between 4 and 30° to homogenize the size of the resultant D-HDL complexes [38]. Analysis of the products by polyacrylamide gradient gel electrophoresis (PAGGE) [39] in 4-24% gels indicated that all the preparations of the differently labeled proteins (or protein mixtures) generated homogeneous D-HDL with a predominant population of complexes with an apparent diameter of about 8 nm or 140 kDa. The emission maxima of tryptophan fluorescence were very similar in all D-HDL preparations.

2.6 Fluorescence measurements.

Fluorescence spectra and anisotropy measurements were made in cells of 0.2 cm path length for excitation and 1 cm for emission using an Olis upgraded SLM4800 spectrofluorometer (Olis Inc., Bogart, GA). Fluorescence spectra were taken with a resolution of 4 nm for excitation and emission. Excitation wavelengths were respectively 290, 350 and 490 nm for tryptophan, Alexa-350 and Alexa-488. A T format was used for anisotropy measurements; observing the emission light through cut-off filters KV389 and KV510 for Alexa-350 and Alexa-488, respectively. D-HDL preparations with 100% wild type apoA-I were used for background subtractions of scattering and non-specific fluorescence.

2.7 Cell cholesterol efflux measurements.

Raw 264.7 macrophagues were cultured as previously described [40]. About 5×10^5 cells were seeded on six-well plates and incubated until confluence (1 day) with 2ml of Dulbecco's Modified Eagle Medium (DMEM) supplemented with penicillin/streptomycin (100 units/ml) and 10% FBS at 37 °C in a 5% CO_2 atmosphere. For cholesterol efflux measurements, RAW 264.7 cells were labeled loaded with 50 mg/ml cholesterol in DMEM and 0.05 mCi/ml 14[C] cholesterol (Perkin Elmer) supplemented with 1% fatty acid-free bovine albumin for 24 h. Following the labeling period, cells were washed twice with PBS and allowed to equilibrate in culture medium containing 1 mg/ml BSA in the presence of 0.5mM Br-cAMP. After 8 h equilibration, cells were washed and incubated for additional 12 h in DMEM with increasing doses of D-HDL maintaining the stimulus of Br-cAMP. Background efflux was determined in control cells incubated with serum-free medium. Efflux media were collected and centrifuged to remove any detached cells and counted for 14C. Then, cells were scraped and suspended in methanol. Cholesterol

efflux was calculated as the percentage of radioactivity in the medium relative to total radioactivity in cells plus medium as previously described [41].

3. THEORY/CALCULATION

3.1 Homo- and hetero-FRET. Dependence on the interprobe distance.

FRET efficiency (E_T) depends on the average distance (R) between two identical (homo-FRET) or two different (hetero-FRET) fluorescent groups according to:

$$E_T = 1 / [1 + (R / R_O)^6] \quad (1)$$

where R_O (or Föster distance) is the distance for $E_T = 0.5$ and it can be calculated (in nm) as:

$$R_O = 0{,}0211 (n^{-4} \kappa^2 Q_D J_{(\lambda)})^{1/6} \quad (2)$$

where n is the refractive index (taken as 1.4), κ^2 is the orientation factor (assumed to be 2/3 for randomly oriented donor and acceptor). Q_D is the donor quantum yield in the absence of FRET and $J_{(\lambda)}$ is the spectral overlap integral calculated as:

$$J_{(\lambda)} = \int f_{D(\lambda)} \varepsilon_{A(\lambda)} \lambda^4 \, d\lambda \quad (3)$$

where $f_{D(\lambda)}$ is the donor emission spectrum with area normalized to unity, $\varepsilon_{A(\lambda)}$ is the absorption spectra of the acceptor at 1 M concentration, and λ is the wavelength.

For hetero-FRET, the efficiency E_T can be calculated from the increase in donor fluorescence intensity, or from the decrease in the acceptor fluorescence intensity or lifetime. In the last case:

$$E_T = 1 - (\tau_{DA} / \tau_D) = 1 - (Q_{DA} / Q_D) = 1 - (F_{DA} / F_D) \quad (4)$$

where τ_{DA} and τ_D are, respectively, the donor fluorescence lifetimes in the presence and absence of acceptor, while Q_{DA} and Q_D are the corresponding donor quantum yields. The quantum yield ratio Q_{DA}/Q_D can be replaced by the equivalent ratio of fluorescence intensities F_{DA}/F_D. By combining equations 1 and 4, the following expression is obtained which permits to calculate the interprobe distance R from fluorescence intensity or lifetime measurements.

$$R = R_O [\tau_{DA} / (\tau_D - \tau_{DA})]^{1/6} = R_O [Q_{DA} / (Q_D - Q_{DA})]^{1/6} = R_O [F_{DA} / (F_D - F_{DA})]^{1/6} \quad (5)$$

In the case of a pure homo-FRET process, it does not change lifetime or quantum yield, but it results in a decrease of the fluorescence anisotropy. Two approximate expressions have been derived to estimate the interprobe distance from steady state anisotropy data [42-44]:

$$R = R_O [0{,}5 \text{ x } (2 r_2 - r_{1)} / (r_1 - r_2)]^{1/6} \quad (6)$$

or

$$R = R_O [(2 r_2 - r_1) / (r_1 - r_2)]^{1/6} \quad (7)$$

where r_1 and r_2 are the anisotropies either in absence or presence of homo-FRET, respectively. We herein used equation 7, which results in 12% longer values for R in comparison with equation 6.

3.2 Self-quenching efficiency.

When interprobe distance is short enough, a self-quenching phenomenon is possible due to the formation of dimeric dark complexes [42]. Like hetero-quenching, self-quenching may or may not affect the fluorescence lifetime. In any case, it will decrease the fluorescence intensity according to:

$$E_{SQ} = 1 - (Q_{SQ} / Q_O) = 1 - (F_{SQ} / F_O) \quad (8)$$

where E_{SQ} is the self-quenching efficiency, Q_{SQ} and Q_O (or F_{SQ} and F_O) are the quantum yields (or relative fluorescence intensities) in the presence and absence of self-quenching, respectively.

In dimeric D-HDL preparations, E_{SQ} could be estimated if we know the ratio of quantum yields or specific fluorescence intensities between D-HDL particles containing two fluorescently labeled apoAI molecules (LL discs) and particles containing one labeled and one unlabeled wild type apoAI molecule (LU discs):

$$E_{SQ} = 1 - (Q_{LL} / Q_{LU}) = 1 - (F_{LL} / F_{LU}) \quad (9)$$

Q_{LL} (or F_{LL}) values can be directly obtained from intensity measurements in a preparation of LL discs, reconstituted with 100% of the labeled protein L. On the contrary, it is not possible to obtain LU discs in a homogeneous state. If a mixture of labeled (L) and unlabeled (U) proteins is used in the reconstitution, a

mixture of discs with the three possible combinations is expected (LL, LU and UU). If there is no preferential interaction, the distribution of them will be:

$$f_{LL} = f_L^2, \qquad f_{LU} = 2\, f_L\, f_U = 2\, f_L\, (1\text{-}f_L), \qquad \text{and } f_{UU} = f_U^2 = (1\text{-}f_L)^2 \tag{10}$$

where f_{LL}, f_{LU} and f_{UU} are the molar fractions of the resultant LL, LU and UU discs; while f_L and f_U=1-f_L, are the molar fractions of L and U in the initial mixture. Starting from an equimolar mixture of L and U, the expected distribution will be 25% of LL, 50% of LU and 25% of UU discs.

Since the UU species is non-fluorescent, and LL contains twice more fluorescent groups than LU, the total fluorescence intensity (F_T) of a D-HDL preparation reconstituted with a mixture of L and U will be:

$$F_T = 2\, (f_{LL}\, Q_{LL} + f_{LU}\, Q_{LU})\, [P_T] = 2\, (f_L^2\, Q_{LL} + f_L\, (1\text{-}f_L)\, Q_{LU})\, [P_T] \tag{11}$$

where $[P_T] = [L] + [U]$, is the total protein concentration in the sample.

Factor 2 may be ignored since fluorescence intensity units are relatives. Moreover, if the fluorescence intensity is normalized (F_N) by the concentration of labeled protein $[L] = f_L\, [P_T]$,

$$F_N = F_T / [L] = f_L\, Q_{LL} + (1 - f_L)\, Q_{LU} = Q_{LU} + f_L\, (Q_{LL} - Q_{LU}) \tag{12}$$

Dividing by Q_{LL}, the following function is obtained which allows to obtain the ratio of quantum yields either in the absence or of self-quenching from the origin ordinate of plots of F_N/Q_{LL} versus f_L:

$$F_N / Q_{LL} = f_L\, (1 - Q_{LU} / Q_{LL}) + (Q_{LU} / Q_{LL}) \tag{13}$$

Once the value for the origin ordinate (Or) is obtained, E_{SQ} can be calculated from the following expression that is equivalent to equation 9:

$$E_{SQ} = 1\text{-}(1 / Or) \tag{14}$$

3.3 Homo-FRET measurements in dimeric D-HDL.

For the case of dimeric D-HDL, r_2 in equations 6 and 7 corresponds to the anisotropy of D-HDL LL (r_{LL}) and r_1 to the anisotropy of D-HDL LU (r_{LU}). While r_{LL} can be directly measured in D-HDL reconstituted with 100% of L, r_{LU} should be indirectly calculated from measurements in D-HDL preparations containing L and U in different proportions. The total anisotropy (r_T) of a D-HDL preparation with a determined molar fraction of L (f_L) will be:

$$r_T = [f_L\, Q_{LL}\, r_{LL} + (1 - f_L)\, Q_{LU}\, r_{LU}] / [f_L\, Q_{LL} + (1 - f_L)\, Q_{LU}] \tag{15}$$

In the absence of self-quenching $Q_{LL} = Q_{LU}$, and this equation simplifies to:

$$r_T = r_{LU} + f_L\, (r_{LL} - r_{LU}) \tag{16}$$

In the presence of self-quenching with efficiency E_{SQ}, Q_{LL} in equation 15 can be replaced by its equivalent $(1 - E_{SQ})\, Q_{LU}$ (see equation 9):

$$r_T = [f_L\, (1 - E_{SQ})\, r_{LL} + (1 - f_L)\, r_{LU}] / (1 - f_L\, E_{SQ}) \tag{17}$$

Multiplying by $(1 - f_L\, E_{SQ})$ and reordering:

$$r_T\, (1 - f_L\, E_{SQ}) = r_{LU} + f_L\, [(1 - E_{SQ})\, r_{LL} - r_{LU}] \tag{18}$$

Estimating E_{SQ} from intensity measurements, and plotting $r_T\, (1 - f_L\, E_{SQ})$ versus f_L, r_{LU} can be obtained from the origin ordinate.

Figure S-1 in Supplemental Data shows the influence of self-quenching on the r_T versus f_L plots. It is to note that the influence of self-quenching can be neglected when $E_{SQ} \leq 0.2$.

3.4 Hetero-FRET measurements in dimeric D-HDL.

Based on the same considerations given above, in a D-HDL preparation reconstituted with an equimolar mixture of donor D and acceptor, it is to expect that 25% of D-HDL particles will contain only donor (DD), 25% will contain only acceptor (AA), and 50% of the particles will contain donor and acceptor (DA). The total fluorescence intensity (Ft_{DA}) of the sample will be:

$$Ft_{DA} = 0.5\, Q_{DD} + 0.5\, Q_{DA} \tag{19}$$

where Q_{DD} is the quantum yield (or specific emission intensity) of D in DD discs, while Q_{DA} is the donor quantum yield in DA discs.

Similarly, the total fluorescence (Ft_{DU}) of a D-HDL preparation reconstituted with a 1/1 molar ratio of D and the unlabeled protein U is:

$$Ft_{DU} = 0.5\, Q_{DD} + 0.5\, Q_{DU} \tag{20}$$

where Q_{DU} is the D quantum yield in DU discs and Q_{DD} was above defined.

The hetero-FRET efficiency will be given by $E_T = 1- (Q_{DA} / Q_{DU})$, while the self-quenching efficiency (defined above) will be $E_{SQ} = 1- (Q_{DD} / Q_{DU})$. By combining these relationships with equations 19 and 20, the following expression is obtained:

$$E_T = [1 - (Ft_{DA} / Ft_{DU})] (2-E_{SQ}) \quad (21)$$

This expression permits to calculate E_T from the measurable total intensities Ft_{DA} and Ft_{DU} and the self-quenching efficiency E_{SQ} independently determined as above explained. It must be noted that in absence of self-quenching equation 21 is reduced to:

$$E_T = 2 [1 - (Ft_{DA} / Ft_{DU})] \qquad \text{for } E_{SQ} = 0 \quad (22)$$

4. RESULTS

4.1 Measurements with single tryptophan mutants.

The single tryptophan mutants W@104 and W@108 were used for preparing D-HDL of DMPC using the CD and DM method. After applying the described temperature cycling, all the samples showed a single band of about 140 kDa or 8 nm in Stokes diameter (not shown). Tryptophan fluorescence spectra and anisotropies were measured. Wavelength of emission maxima, relative intensities and anisotropy values are given in table I. For both mutants, a decrease in the relative intensity or quantum yield as well as in the anisotropy was observed in D-HDL DM in comparison with D-HDL CD. The decrease in intensity indicates the presence of self-quenching in DM samples suggesting that in these discs the intermolecular distance between Trp residues is short enough to allow the formation of dark complexes. The big change in anisotropy detected between CD and DM samples exceeds the one predicted by a maximal change of FRET efficiency from 0 in D-HDL CD to 1 in D-HDL DM. Then, considering that R_O for Trp-Trp homo-FRET is about 1 nm [34], the average intermolecular 104-104 and 108-108 distances should be ≤ 0.6 nm in D-HDL DM and ≥ 1.7 nm in D-HDL CD (i.e. the sensitivity limits given by $0.6\ R_O$ and $1.7\ R_O$, respectively. See below). If these results are interpreted according to the 5/5 and 5/2 configurations proposed by Silva et al. [27], they suggest that the 5/5 registry predominates in D-HDL prepared by the CD method while the 5/2 registry prevails in those D-HDL generated by the DM method.

4.2 Measurements with cysteine mutants.

4.2.1 Mutants and probes selection.

In order to confirm if the DM method generates D-HDL in the 5/2 configuration in opposition to the CD method, we have constructed three cysteine mutants (K107C, K133C and K226C) which were specifically designed to distinguish between 5/5 and 5/2 orientational arrangements. These positions in the polar faces of helices 4, 5 and 10, respectively, were selected considering that the intermolecular 107-107 and 133-133 distances will suffer the maximal change between both configurational arrangements. As illustrated in figure 1, the intermolecular distance between residues 107 is much shorter in the 5/2 than in the 5/5 registry, while the opposite is true for the 133-133 distance. The intermolecular distance 226-226, on the other hand, is maintained approximately constant in both orientations and will serve as a negative control. Considering the size of D-HDL (8 nm diameter) and predicted distance changes in both orientational arrangements, fluorescent probes (and probe pairs) were selected having adequate Föster distances (R_O) for homo- and hetero-FRET detection in the distance range from about 1 to 9 nm (see table S-III in supplemental data).

4.2.2 Homo-FRET measurements in D-HDL DM reconstituted with Alexa-488 labeled cysteine mutants.

Firstly, we labeled the cysteine mutants with Alexa-488 to estimate the intermolecular distances in D-HDL reconstituted by the DM method in order to confirm if these D-HDL display the 5/2 configuration as suggested by the measurements with single tryptophan mutants. For this, D-HDL were reconstituted by the DM method with the Alexa-488-labeled mutants in mixtures with different proportions of the unlabeled wild type protein. Alexa-488 fluorescence intensity measurements indicated that self-quenching was present only in the case of D-HDL prepared with the mutant labeled in position 107 ($E_{SQ} \approx 10\%$), but not in D-HDL prepared with the other mutants (data not shown). Since self-quenching has no appreciable

influence when $E_{SQ} \leq 20\%$ (see figure S-1 in Supplemental Data), it was neglected and equation 16 was directly used for anisotropy data interpretation. Measured anisotropy values are plotted in figure 2 as a function of the molar fraction of labeled protein (f_L). It is to note that anisotropy values were relatively low, indicating a high mobility of the Alexa-488 group. This fact allows the assumption of a random orientation of fluorescent groups and justifies the use of 2/3 for the orientational factor κ^2 in R_O calculations. From the origin ordinates and slopes of plots in figure 2, the anisotropy values in the absence (r_{LU} or r1) and presence (r_{LL} or r2) of homo-FRET were calculated and given in the figure insert. Equation 7 was then used for estimating the average intermolecular distances, which are given in table III. Considering the size of Alexa-488 group (see below), the estimated 133-133 distance (4.8 nm) is compatible with a double belt in the 5/2 helix registry. The 107-107 and 226-226 distances were too short in comparison with R_O for Alexa-488 homo-FRET to allow a precise estimation, but this fact is even compatible with the 5/2 orientation.

4.2.3. Self-quenching and homo-FRET measurements in D-HDL reconstituted with Alexa-350-labeled cysteine mutants.

Since R_O for homo-FRET in Alexa-350 is considerably lower than in Alexa-488 (see table S-III), this probe was used for determining the intermolecular distances that could not be precisely estimated by Alexa-488 homo-FRET. D-HDL were reconstituted by CD and DM approaches with the three Alexa-350 labeled mutants mixed with different proportions of the wild type protein (f_L = 0.25, 0.5 and 1). The Alexa-350 fluorescence intensity for each D-HDL preparation (normalized by the intensity of the same sample after treatment with 3 M GdnHCl as well as the intensity of the samples with f_L=1) is shown in figure 3 plotted versus the molar fraction of the labeled protein. These plots follow the function described by equation 13. Then, the ratio between the quantum yields in the absence and presence of self-quenching (Q_{LU}/Q_{LL}), and self-quenching efficiencies (E_{SQ}) can be obtained for the origin ordinates. The values, given in the insert of figure 3, indicate a high efficiency of self-quenching for CD reconstituted D-HDL of the mutant labeled at position 133 (65%) and for DM D-HDL in the case of the mutant labeled at position 107 (50%). Concerning the protein labeled in position 226, a low self-quenching efficiency (15%) is detected in D-HDL DM. These data indicate that when the labeled position is 133, the fluorescent groups are close together allowing the formation of dark complexes in the D-HDL prepared by the CD method, fact that is compatible with a major proportion of the 5/5 configuration. On the contrary, the self-quenching detection for DM D-HDL when the labeled position is 107 is compatible with the 5/2 configuration.

The anisotropy data, modified as rt (1- f_L E_{SQ}), are shown in figure 4 plotted versus the molar fraction of labeled protein (f_L). By fitting equation 18 to these data, the anisotropies in the absence (rt_{LU} o r1) or presence (rt_{LL} o r2) of homo-FRET were calculated. They are shown in the figure insert, while the estimated intermolecular distances between the labeled positions are given in table III. These data indicate that the intermolecular 107-107 distance in DM D-HDL is about 0.9 nm, but it is higher than 2.2 nm in CD D-HDL. Residues 133, on the contrary, are separated each other by about 0.8 nm in the D-HDL prepared by the CD method, but by about 1.8 nm in DM prepared D-HDL. On the other hand, the intermolecular distance between residues 226 is estimated to be 1.7 nm in D-HDL prepared by both methods.

With the exception of the 133-133 distance in DM D-HDL, which is considerably shorter when detected by Alexa-350 (1.8 nm) than by Alexa-488 homo-FRET (4.8 nm), data are qualitatively in agreement and support the hypothesis that the major configuration in these D-HDL is the 5/2 registry. Together with self-quenching data, Alexa-350 homo-FRET indicates that, on the contrary, the major configuration of apoAI in D-HDL prepared by the CD method is the 5/5 orientation.

4.2.4 Hetero-FRET measurements with Alexa-350 as donor, and Alexa-488 or Alexa-647 as acceptors.

For hetero-FRET measurements, D-HDL were reconstituted by both methods (DM and CD) starting with mixtures (1/1 in molar ratio) of each one of the mutants labeled with Alexa-350 (donor D) with the corresponding mutants labeled with Alexa-488 or Alexa-647 (acceptors A), or with wild type apoAI

(unlabeled U). PAGGE controls indicated that all the resulting D-HDL were about 8 nm diameter and tryptophan fluorescence spectra did not detect any spectral shift discarding the possibility of an altered folding evoked by the label (not shown). Alexa-350 emission spectra (excitation at 350 nm) were registered before and after mixing the samples with the same volume of 6.0 M GdnHCl (3.0 M final concentration).

Typical spectra obtained before the addition of GdnHCl are shown in supplemental data (figure S-2). Hetero-FRET results in an increased acceptor emission that disappears in 3 M GdnHCl. Hetero-FRET also results in the decrease of the donor Alexa-350 fluorescence emission intensity, fact that was herein used for quantifying the hetero-FRET efficiencies. The integral of the spectra (between 390 and 480 nm) in the absence of GdnHCl was divided by the corresponding integral in the presence of GdnHCl to obtain the values of total intensities Ft_{DA} (in samples containing donor and acceptor) or Ft_{DU} (in samples containing donor and unlabeled wild type protein), corresponding to equations 19 and 20. The ratios Ft_{DA}/Ft_{DU} are shown in table II together with hetero-FRET efficiencies (Et) calculated from equation 21. The intermolecular distances (R) estimated from equation 5 are given in table III. The obtained data clearly indicate that the average 107-107 intermolecular distance is much shorter in DM D-HDL than in CD D-HDL. On the contrary, the 133-133 intermolecular distance is much shorter in CD D-HDL than in DM D-HDL. The intermolecular distance between residues 226, on the other hand, does not change too much between both reconstitution methods. Thus, also these results support the hypothesis that apoAI configuration in DM D-HDL is mostly the 5/2 registry, while that one in CD D-HDL is the 5/5 orientation.

4.3 Functional properties of D-HDL DM and CD. Cholesterol efflux from cell cultures.

The results obtained with single tryptophan and cysteine mutants of apoAI showed that apoAI configuration in D-HDL depends on the method used in their reconstitution. In order to know if the different configuration of apoAI in D-HDL prepared by DM and CD methods is relevant for the functional properties of D-HDL, the capacity to promote cholesterol efflux from cultured macrophages was compared. Confluent cultures of RAW 264.7 macrophages were loaded with cholesterol as described in Experimental Procedures Section. Then, cells were treated with different concentrations of CD and DM D-HDL for 12 h. In this experiment, CD and DM D-HDL reconstituted with recombinant and serum apoA-I were compared. After treatment, radioactivity was counted in the medium and cell monolayers. Cholesterol efflux, expressed as percentage of radioactivity in the medium with respect to the total radioactivity incorporated in cell is plotted in figure 5 versus the concentration of D-HDL added in the medium. It was found that D-HDLs reconstituted with recombinant or serum apoA-I have a similar behavior indicating that the lack of two residues at the N terminal does not affect its functionality. The D-HDL activity, however, was dependent on the reconstitution method. At low D-HDL concentrations ($\leq$ 10 μg/ml), the activity of those prepared by the DM method was higher than that of those prepared by the CD method. At high concentrations, however, the activity of CD D-HDL was similar or somewhat higher than that of DM D-HDL.

5. DISCUSION

In this work, we have shown that the configuration of apoAI in reconstituted D-HDL depends on the method used for their preparation. The measurements with the single tryptophan mutants W@104 and W@108 indicated that the intermolecular distances between homologous residues 104-104 and 108-108 are much shorter in DM D-HDL than in CD D-HDL, leading in the first case to self-quenching and decreased anisotropy of tryptophan fluorescence. More precise distance estimations could be obtained by using the cysteine mutants K107C, K133C and K226C labeled with different fluorophores in order to span a wide range of R_O values and distance sensitivity through homo- and hetero-FRET measurements. Table III summarizes the intermolecular distances and distance constraints between homologous residues (107-107, 133-133 and 226-226) obtained for both kinds of reconstituted samples (CD and DM D-HDLs). For comparison, table II also shows the intermolecular distances between Cα of these residue pairs in the crystal structure of apoAI Δ1-43 (which can be taken as a reference for the 5/5 registry) and those

distances arising from the displacement for 5 nm of an apoAI ring with respect to the other (as an approximate reference for the 5/2 orientation).

There is an acceptable concordance between the distances reported by the different probes or probe pairs, with the only exception of homo-FRET with Alexa-350 which tends to report shorter distances than other probes. Considering the size of the probes and that they can be differently oriented at their cysteine attachment sites, the average effective distances measured by FRET can differ almost 2 nm from those between the Cα of the corresponding residues [45]. Taking this fact into account, the 133-133 and 226-226 intermolecular distances measured by FRET in CD D-HDL are in good agreement with those in the crystal structure of apoAI Δ1-43 and thus with the expected distances in the 5/5 orientation. For the 107-107 distance, however, FRET reported a considerably shorter distance than that between the Cα in the apoAI Δ1-43 crystal. This fact could be explained by a probe orientation at the cys attachment size resulting in the approaching of fluorescent groups and lower effective distance for FRET. However, it also can be due to the coexistence of a minor proportion of discs having the 5/2 registry as it was detected by Silva et al. [27] in D-HDL reconstituted with POPC through the CD method.

With regard to DM D-HDL, there is good agreement between the intermolecular distances measured by FRET with those expected for the 5/2 orientation, with the exception of the 133-133 distance measured by homo-FRET with Alexa-350 which is shorter than the expected one. With all probes and probe pairs, the measured intermolecular distance 107-107 was shorter in DM D-HDL than in CD D-HDL, while the opposite was true for the 133-133 distance and no large changes were observed for the distance between residues 226. Although alternative configurations cannot be discarded, data indicate that most of the D-HDL prepared by the DM method present the 5/2 registry while most of the discs prepared by CD present the 5/5 orientation. Detection of self-quenching of Alexa-350 in DM D-HDL with the mutant labeled in position 107, and in CD D-HDL with the mutant labeled in 133 also indicates that the DM method preferentially generates the 5/2 registry while the CD method preferentially generates the 5/5 orientation.

The microsolubilization reaction at the phase transition temperature of phospholipid vesicles is attributed to the coexistence of fluid and gel lipid domains, fact that generates bilayer packing defects at the domain interfaces [13]. The reaction follows a second order kinetics and consists of two simultaneous kinetic phases [46]. The two kinetic components were proposed to arise from two distinct types of binding sites (with or without lattice defects) for apoAI on the vesicle surface. If the initial apoA-I/MLV contact occurs at a packing defect in the DMPC bilayer surface, then the reaction proceeds directly. Initial contact at a non-defect site, however, will require diffusion of the apoAI molecule over the surface until reaching a defect site, giving rise to the slow kinetic phase. In any case, the reaction requires the initial binding of apoAI to the vesicle surface which is a reversible process, contrarily to the conversion in D-HDL that is irreversible. As shown in previous reports, the membrane bound state of apoAI is essentially dimeric [47], and it occurs with the deep insertion in the lipid bilayer of the central 3-4 helix pair [10] whereas the rest of the helices interact more superficially. The determination of the insertion topology of the 3-4 helix pair in the lipid bilayer [34] allowed the proposal of a model in which an intermolecular bundle of both central helix pairs of the dimeric apoAI penetrates one leaflet of the lipid bilayer with the helix axis perpendicular to the membrane surface. The particular distribution of charged residues at the polar faces of these helices would allow the bundle stabilization through saline bridges. Dimerization of apoAI in aqueous solution also seems to be the result of interactions between the 3-4 helix pairs, although in this case through the hydrophobic helix faces [34]. Then, the apoAI dimerization through the intermolecular interaction of the 3-4 helix pairs, either before or after binding to the membrane, can determine the final configuration of the DM generated D-HDL, whose apoAI molecules would remain aligned or juxtaposed in the region of the 3-4 helix pairs and thus in the 5/2 registry (see figure 1).

On the other hand, the formation of mixed apoAI/phospholipid/cholate micelles would not require previous dimerization of apoAI. When cholate is progressively removed by dialysis, apoAI helices would replace it at the edge of the lipid bilayer disc patch. In this case, the determinant for intermolecular helix-helix interactions and the preferred 5/5 configuration would be the maximization of saline bridges as it occurs in the apoAI Δ1-43 crystal [21], as proposed by Segrest [17] in the development of the double belt model.

The fact that both apoAI configurations (5/5 and 5/2 registries) can be generated by independent procedures implies the existence of a thermodynamic barrier for their interconversion. In this respect, molecular dynamics simulations were made with D-HDL models starting from configurations similar to that of the apoA-I Δ1-43 crystal but differing in the initial alignment by a helix turn (G129/G129 or K133/K133 rotamers). Breaking and reformation of saline bridges were observed in a time scale of 100 ps allowing the rotation of an apoAI molecule with respect to the other [48]. However, rotation stopped when proline residues of both molecules (which are regularly spaced in the sequence) becomes juxtaposed and stacked. The protein double belt, initially circular, acquired then a hexagonal shape with straight helix stretches interrupted at the stacked proline pairs. Based on this observation, it was proposed that proline-induced kinking introduces a kinetic barrier to the rotation of two apo A-I monomers on an HDL disk.

As proposed [3, 13], the "in vivo" generation of nascent D-HDL mediated by the ABCA1 transporter at the cell membrane would occur by a mechanism basically similar to the direct microsolubilization of phospholipid vesicles at the phase transition. Thus, it is probable that "in vivo" generated D-HDL by the action of ABCA1 would present the same major configuration (5/2 registry) as those D-HDL generated by the microsolubilization of DMPC vesicles at 24°C. This possibility must be confirmed, but it is worth noting that evidence obtained by cross-linking indicates that both, the 5/2 and 5/5 registries are present in natural HDL complexes [28, 29].

In this work, we have also shown that the reconstitution method (CD or DM) impacts on the activity of the resulting D-HDL to remove cholesterol from RAW macrophages, suggesting that helix registry could be important for this activity. As noted above, cell cholesterol efflux evoked by apoAI and its lipoprotein complexes can occur through different mechanisms either independent or dependent on cellular transporters as ABCA1, ABCG1 and SRB1. ApoAI configuration in D-HDL may be important for recognition of cellular proteins as well as for the direct interaction with specific lipid domains of the cell membrane. D-HDL can bind to protein-free lipid vesicles [33,49,50], and this interaction facilitates cholesterol exchange between vesicles and D-HDL [9]. As it happens with lipid-free apoAI, binding of D-HDL to lipid vesicles seems to occur with the deep insertion into the vesicle lipid bilayer of the central apoAI region consisting of helices 3 and 4 [10]. This fact indicates that the intermolecular helix bundle proposed as the membrane inserting domain [34] should be also operative in the case of D-HDL. It is to note that the formation of this intermolecular 4-helix bundle within a D-HDL particle is only possible with the 5/2 double belt configuration but not with the 5/5 registry (see figure 1). Thus, it is likely that the increased cell cholesterol efflux evoked at low concentrations by DM D-HDL in comparison with CD D-HDL could be due to the fact that the 5/2 registry predominates in the first case. At high D-HDL concentrations, other mechanisms independent of the apoAI double-belt registry as the aqueous diffusion pathway could be predominant.

6. CONCLUSIONS

In summary, the present results show that the reconstitution method affects both apoAI configuration and kinetics of cell cholesterol removal of D-HDL. Although alternative configurations cannot be discarded, the results can be explained by the predominance of the 5/2 configuration in DM D-HDL and of the 5/5 registry in D-HDL prepared by the CD method. Further experiments are needed to clearly determine the apoAI configuration and helix registry in natural D-HDL as well as to know their importance for HDL functionality in the RCT and other antiatherogenic processes mediated by this protein.

ACKNOWLEDGEMENTS

This work was supported by grants from Consejo Nacional de Investigaciones Científicas y Técnicas (CONICET), Agencia Nacional de Promoción Científica y Tecnológica (ANPCyT), and Universidad Nacional de La Plata. HAG is member of the scientific research career of CONICET, while LAC and

EDP are fellows from the same institution. Authors acknowledge Mrs. Laura Hernandez for her expert technical assistance and Mrs. Rosana del Cid and Norma Tedesco for English revision and editing.

REFERENCES

[1] G.H. Rothblat, M.C. Phillips, High-density lipoprotein heterogeneity and function in reverse cholesterol transport, Curr. Opin. Lipidol. 21 (2010) 229-238.
[2] M.H. Kang, R. Singaraja, M.R. Hayden, Adenosine-triphosphate-binding cassette transporter-1 trafficking and function, Trends Cardiovasc. Med. 20 (2010) 41-49.
[3] C. Vedhachalam, P.T. Duong, M. Nickel, D. Nguyen, P. Dhanasekaran, H. Saito, G.H. Rothblat, S. Lund-Katz, M.C. Phillips, Mechanism of ATP-binding cassette transporter A1-mediated cellular lipid efflux to apolipoprotein A-I and formation of high density lipoprotein particles, J. Biol. Chem. 282 (2007) 25123-25130.
[4] P.T. Duong, G.L. Weibel, S. Lund-Katz, G.H. Rothblat, M.C. Phillips, Characterization and properties of pre beta-HDL particles formed by ABCA1-mediated cellular lipid efflux to apoA-I, J. Lipid Res. 49 (2008) 1006-1014.
[5] I.C. Gelissen, M. Harris, K.A. Rye, C. Quinn, A.J. Brown, M. Kockx, S. Cartland, M. Packianathan, L. Kritharides, W. Jessup, ABCA1 and ABCG1 synergize to mediate cholesterol export to apoA-I, Arterioscler. Thromb. Vasc. Biol. 26 (2006) 534-540.
[6] M. Hoekstra, T.J. Van Berkel, M. Van Eck, Scavenger receptor BI: a multi-purpose player in cholesterol and steroid metabolism, World J. Gastroenterol. 16 (2010) 5916-5924.
[7] M.P. Adorni, F. Zimetti, J.T. Billheimer, N. Wang, D.J. Rader, M.C. Phillips, G.H. Rothblat, The roles of different pathways in the release of cholesterol from macrophages, J. Lipid Res. 48 (2007) 2453-2462.
[8] M.C. Phillips, W.J. Johnson, G.H. Rothblat, Mechanisms and consequences of cellular cholesterol exchange and transfer, Biochim. Biophys. Acta. 906 (1987) 223-276.
[9] J.D. Toledo, M.A. Tricerri, B. Córsico, H.A. Garda, Cholesterol flux between lipid vesicles and apolipoprotein AI discs of variable size and composition, Arch. Biochem. Biophys. 380 (2000) 63-70.
[10] B. Córsico, J.D. Toledo, H.A. Garda, Evidence for a central apolipoprotein A-I domain loosely bound to lipids in discoidal lipoproteins that is capable of penetrating the bilayer of phospholipid vesicles, J. Biol. Chem. 276 (2001) 16978-16985.
[11] L. Calabresi, G. Franceschini, Lecithin:cholesterol acyltransferase, high-density lipoproteins, and atheroprotection in humans, Trends Cardiovasc. Med. 20 (2010) 50-53.
[12] C.E. Matz, A. Jonas, Micellar complexes of human apolipoprotein A-I with phosphatidylcholines and cholesterol prepared from cholate-lipid dispersions, J. Biol. Chem. 257 (1982) 4535-4540.
[13] S. Lund-Katz, M.C. Phillips, High density lipoprotein structure-function and role in reverse cholesterol transport, Subcell. Biochem. 51 (2010) 183-227.
[14] J.H. Wald, E. Coormaghtigh, J. De Meutter, J.M. Ruysschaert, A. Jonas, Investigation of the lipid domains and apolipoprotein orientation in reconstituted high density lipoproteins by fluorescence and IR methods, J. Biol. Chem. 265 (1990) 20044-20050.
[15] C.G. Brouillette, G.M. Anantharamaiah, Structural models of human apolipoprotein A-I, Biochim. Biophys. Acta. 1256 (1995) 103-129.
[16] C.G. Brouillette, G.M. Anantharamaiah, J.A. Engler, D.W. Borhani, Structural models of human apolipoprotein A-I: a critical analysis and review, Biochim. Biophys. Acta. 1531 (2001) 4-46.
[17] J.P. Segrest, M.K. Jones, A.E. Klon, C.J. Sheldahl, M. Hellinger, H. De Loof, S.C. Harvey, A detailed molecular belt model for apolipoprotein A-I in discoidal high density lipoprotein, J. Biol. Chem. 274 (1999) 31755-31758.
[18] A.E. Klon, J.P. Segrest, S.C. Harvey, Comparative models for human apolipoprotein A-I bound to lipid in discoidal high-density lipoprotein particles, Biochemistry. 41 (2002) 10895-10905.
[19] V. Koppaka, L. Silvestro, J.A. Engler, C.G. Brouillette, P.H. Axelsen, The structure of human lipoprotein A-I. Evidence for the “belt” model, J. Biol. Chem. 274 (1999) 14541-14544.
[20] S.E. Panagotopulos, E.M. Horace, J.N. Maiorano, W.S. Davidson, Apolipoprotein A-I adopts a belt-like orientation in reconstituted high density lipoproteins, J. Biol. Chem. 276 (2001) 42965-42970.

[21] D.W. Borhani, D.P. Rogers, J.A. Engler, C.G. Brouillette, Crystal structure of truncated human apolipoprotein A-I suggests a lipid-bound conformation, Proc. Natl. Acad. Sci. U. S. A. 94 (1997) 12291-12296.
[22] L.A. Schneeweis, V. Koppaka, S. Lund-Katz, M.C. Phillips, P.H. Axelsen, Structural analysis of lipoprotein E particles, Biochemistry. 44 (2005) 12525-12534.
[23] R.A. Silva, L.A. Schneeweis, S.C. Krishnan, X. Zhang, P.H. Axelsen, S.W. Davidson, The structure of apolipoprotein A-II in discoidal high density lipoproteins, J. Biol. Chem. 282 (2007) 9713-9721.
[24] V. Narayanaswami, J.N. Maiorano, P. Dhanasekaran, R.O. Ryan, M.C. Phillips, S. Lund-Katz, W.S. Davidson, Helix orientation of the functional domains in apolipoprotein E in discoidal high density lipoprotein particles, J. Biol. Chem. 279, 14273-14279.
[25] H.A. Garda, E.L. Arrese, J.L. Soulages, Structure of apolipophorin-III in discoidal lipoproteins. Interhelical distances in the lipid-bound state and conformational change upon binding to lipid, J. Biol. Chem. 277 (2001) 19773-19782.
[26] X. Mei, D. Atkinson, Crystal structure of C-terminal truncated apolipoprotein A-I reveals the assembly of HDL by dimerization, J. Biol. Chem. 286 (2011) 38570-38582.
[27] R.A. Silva, G.M. Hilliard, L. Li, J.P. Segrest, W.S. Davidson, A mass spectrometric determination of the conformation of dimeric apolipoprotein A-I in discoidal high density lipoproteins, Biochemistry 44 (2005) 8600-8607.
[28] R.A. Silva, R. Huang, J. Morris, J. Fang, E.O. Gracheva, G. Ren, A. Kontush, W.G. Jerome, K.A. Rye, W.S. Davidson, Structure of apolipoprotein A-I in spherical high density lipoproteins of different sizes, Proc. Natl. Acad. Sci. U. S. A. 26, (2008) 12176-12181.
[29] R. Huang, R.A. Silva, W.G. Jerome, A. Kontush, M.J. Chapman, L.K. Curtiss, T.J. Hodges, W.S. Davidson, Apolipoprotein A-I structural organization in high-density lipoproteins isolated from human plasma, Nat. Struct. Mol. Biol. 18 (2011) 416-422.
[30] S. Bhat, M.G. Sorci-Thomas, E.T. Alexander, M.P. Samuel, M.J. Thomas, Intermolecular contact between globular N-terminal fold and C-terminal domain of apoA-I stabilizes its lipid-bound conformation. Studies employing chemical cross-linking and mass spectrometry, J. Biol. Chem. 280 (2005) 33015-33025.
[31] W.S. Davidson, T.B. Thompson, The structure of apolipoprotein A-I in high density lipoproteins, J. Biol. Chem. 282 (2007) 22249-22253.
[32] M.G. Sorci-Thomas, J.S. Owen, B. Fulp, S. Bhat, X. Zhu, J.S. Parks, D. Shah, W.G. Jerome, M. Gerelus, M. Zabalawi, M.J. Thomas, Nascent high density lipoproteins formed by ABCA1 resemble lipid rafts and are structurally organized by three apoA-I monomers, J. Lipid Res. 53 (2012) 1890-1909.
[33] M.A. Tricerri, B. Córsico, J.D. Toledo, H.A. Garda, R.R. Brenner, Conformation of apolipoprotein AI in reconstituted lipoprotein particles and particle-membrane interaction: effect of cholesterol, Biochim. Biophys. Acta 1391 (1998) 67-78.
[34] E.D. Prieto, H.A. Garda, Membrane insertion topology of the central apolipoprotein A-I region. Fluorescence studies using single tryptophan mutants, Biochemistry 50 (2011) 466-479.
[35] E.D. Prieto, N. Ramella, L.A. Cuellar, M.A. Tricerri, H.A. Garda, Characterization of a human apolipoprotein A-I construct expressed in a bacterial system, Protein J. 31 (2012) 681-688.
[36] R.O. Ryan, T.M. Forte, M.N. Oda, Optimized bacterial expression of human apolipoprotein A-I, Protein Expr. Purif. 27 (2003) 98-103.
[37] A. Jonas, K.E. Kezdy, J.H. Wald, Defined apolipoprotein A-I conformations in reconstituted high density lipoprotein discs, J. Biol. Chem. 264 (1989) 4818–4824.
[38] L. Li, J. Chen, V.K. Mishra, J.A. Kurtz, D. Cao, A.E. Klon, S.C. Harvey, G.M. Anantharamaiah, J.P. Segrest, Double belt structure of discoidal high density lipoproteins: molecular basis for size heterogeneity, J. Mol. Biol. 343 (2004) 1293-1311.
[39] A.V. Nichols, R.M. Krauss, T.A. Musliner, Nondenaturing polyacrylamide gradient gel electrophoresis, Methods Enzymol. 128 (1986) 417-431.

[40] J.D. Toledo, L.V. Cabaleiro, H.A. Garda, M.C. Gonzalez, Effect of reconstituted discoidal high-density lipoproteins on lipid mobilization in RAW 264.7 and CHOK1 cells, J. Cell. Biochem. 113 (2012) 1208-1216.
[41] M.C. Gonzalez, J.D. Toledo, M.A. Tricerri, H.A. Garda, The central type Y amphipathic alpha-helices of apolipoprotein AI are involved in the mobilization of intracellular cholesterol depots, Arch. Biochem. Biophys. 473 (2008) 34-41.
[42] L.W. Runnels, S.F. Scarlata, Theory and application of fluorescence homotransfer to melittin oligomerization, Biophys. J. 69 (1995) 1569-1583.
[43] B.D. Hamman, A.V. Oleinikov, G.G. Jokhadze, R.R. Traut, D.M. Jameson, Dimer/monomer equilibrium and domain separations of Escherichia coli ribosomal protein L7/L12, Biochemistry 35 (1996) 16680-16686.
[44] P. Zou, K. Surendhran, H.S. Mchaourab, Distance measurements by fluorescence energy homotransfer: evaluation in T4 lysozyme and correlation with dipolar coupling between spin labels, Biophys. J. 15 (2007) L27-L29.
[45] M.A. Tricerri, A.K. Behling Agree, S.A. Sanchez, J. Bronski, A. Jonas, Arrangement of apolipoprotein A-I in reconstituted high-density lipoprotein disks: an alternative model based on fluorescence resonance energy transfer experiments, Biochemistry 40 (2001) 5065-5074.
[46] M.L. Segall, P. Dhanasekaran, F. Baldwin, G.M. Anantharamaiah, K.H. Weisgraber, M.C. Phillips, S. Lund-Katz, Influence of apoE domain structure and polymorphism on the kinetics of phospholipid vesicle solubilization, J. Lipid Res. 43 (2002) 1688-1700.
[47] J.D. Toledo, E.D. Prieto, M.C. Gonzalez, J.L. Soulages, H.A. Garda, Functional independence of a peptide with the sequence of human apolipoprotein A-I central region, Arch. Biochem. Biophys. 428 (2004) 188-197.
[48] A.E. Klon, J.P. Segrest, S.C. Harvey, Molecular dynamics simulations on discoidal HDL particles suggest a mechanism for rotation in the apo A-I belt model, J. Mol. Biol. 324 (2002) 703-21.
[49] M.A. Tricerri, S.A. Sanchez, C. Arnulphi, D.M. Durbin, E. Gratton, A. Jonas, Interaction of apolipoprotein A-I in three different conformations with palmitoyl oleoyl phosphatidylcholine vesicles, J. Lipid Res. 43 (2002) 187-197.
[50] M.A. Tricerri, J.D. Toledo, S.A. Sanchez, T.L. Hazlett, E. Gratton, A. Jonas, H.A. Garda, Visualization and analysis of apolipoprotein A-I interaction with binary phospholipid bilayers, J. Lipid Res. 46 (2005) 669-678.
[51] J.P. Segrest, M.K. Jones, H. De Loof, C. G. Brouillette, Y. V. Venkatachalapathi, G. M. Anantharamaiah, The amphipathic helix in the exchangeable apolipoproteins: a review of secondary structure and function, J. Lipid Res. 33 (1992) 141-166.

Table I. Tryptophan fluorescence parameters for D-HDL prepared with the single tryptophan W@104 and W@108 mutants and DMPC using the cholate-dialysis (CD) and direct microsolubilization (DM) methods.

Mutant	Reconstitution method	λ_{max} (nm)	Relative intensity	Anisotropy	Estimated R (nm)
W@104	CD	341	56	0.117	≥ 1.7
W@104	DM	341	34	0.017	≤ 0.6
W@108	CD	338	100	0.116	≥ 1.7
W@108	DM	340	45	0.049	≤ 0.6

Table II. Hetero-FRET in DM and CD reconstituted D-HDL containing Alexa-350 as donor, and Alexa-488 or Alexa-647 as acceptors. The Ft_{DA}/Ft_{DU} ratio obtained as explained in the text was used for calculating the FRET efficiencies (E_T) using equation 21 and self-quenching efficiencies E_{SQ} given in the insert of figure 3.

Mutant / D-A pair / Method	Ft_{DA}/Ft_{DN}	FRET efficiency (E_T)
M107 / A350-A488 / DM	0.241	> 1.0
M107 / A350-A647 / DM	0.299	> 1.0
M107 / A350-A488 / CD	0.650	0.700
M107 / A350-A647 / CD	0.830	0.340
M133 / A350-A488 / DM	0.840	0.320
M133 / A350-A647 / DM	0.945	0.110
M133 / A350-A488 / CD	0.250	> 1.0
M133 / A350-A647 / CD	0.273	0.978
M226 / A350-A488 / DM	0.645	0.656
M226 / A350-A647 / DM	0.715	0.527
M226 / A350-A488 / CD	0.726	0.548
M226 / A350-A647 / CD	0.855	0.290

Table III. Intermolecular distances (in nm) between residue pairs 107-107, 133-133 and 226-226 estimated by homo- and hetero-FRET measurements in CD and DM D-HDL in comparison with the expected distances in the 5/5 and 5/2 orientations of the double belt.

Residue pair	LL5/5 registry[a]	D-HDL CD			
		Ho A350[c]	He A350/488[d]	He A350/647[e]	Ho A488[f]
107-107	6.4	> 2.2	3.9	3.2	ND[g]
133-133	1.4	0.8	< 2.2	1.5	ND
226-226	2.9	1.7	4.4	3.4	ND
	LL5/2 registry[b]	**D-HDL DM**			
		Ho A350[c]	**He A350/488[d]**	**He A350/647[e]**	**Ho A488[f]**
107-107	1.4	0.9	< 2.2	< 1.4	≤ 2.5
133-133	6.4	1.8	5.1	4.1	4.8
226-226	2.1	1.7	4.0	2.8	≤ 2.5

[a] Cα-Cα distances obtained from the coordinates of the A/B dimer in the crystal structure of apoAI Δ1-43 (21)

[b] Cα-Cα distances arising by supposing a rotation displacing 5 nm one apoAI ring with respect to the other in order to juxtapose helices 5 with helices 2.

[c] Distances obtained by homo-FRET measurements with Alexa-350 labeled proteins

[d] Distances obtained by measurements of hetero-FRET from Alexa-350 to Alexa-488

[e] Distances obtained by measurements of hetero-FRET from Alexa-350 to Alexa-647

[f] Distances obtained by homo-FRET measurements with Alexa-488 labeled proteins

[g] ND = not determined

FIGURE LEGENDS

Figure 1. Schematic diagram illustrating the double-belt arrangement of apoA-I in the 5/5 and 5/2 orientations. Amphipathic α-helices of apoAI are numbered according to Segrest et al. [51] with the G* helix at the N terminal and helices 1 to 10 toward de C end. The approximate localization of residues 107, 133 and 226 are also indicated.

Figure 2. Alexa-488 homo-FRET in D-HDL reconstituted by direct microsolubilization. Alexa-488 steady state fluorescence anisotropy (r_T) was measured in samples of D-HDL prepared by the direct microsolubilization (DM) method with Alexa-488-labeled K107C (circles), K133C (triangles) and K226C (squares) mutants mixed at different molar ratios with unlabeled wild type apoA-I. The means of 5 determinations (and standard deviations) are plotted as a function of the molar fraction of the labeled protein (f_L). The values for the anisotropies in the absence (r_1 or r_{LU}) and in the presence (r_2 or r_{LL}) of homo-FRET, which were calculated from linear regressions of the corresponding plots according to equation 16, are given in the figure insert.

Figure 3. Self-quenching of Alexa-350 fluorescence in reconstituted D-HDL. D-HDL were prepared by the CD (open symbols) and DM (filled symbols) methods, with the mutants labeled with Alexa-350 in position 107 (circles), position 133 (triangles) and position 226 (squares) and mixed in different proportions with unlabeled wild type apoA-I. The fluorescence intensity values normalized by the concentration of labeled protein and the value corresponding to $f_L = 1$ (see text) are plotted as function of the molar fraction of labeled protein (f_L). Data are the means of 3 determinations. Standard deviations are in the order of the symbol size (≤ 0.1 relative fluorescence units). The quantum yield ratio Q_{LU}/Q_{LL} and self-quenching efficiency E_{SQ} calculated from equations 13 and 14 are given in the figure insert.

Figure 4. Alexa-350 homo-FRET in reconstituted D-HDL. D-HDL were prepared by the CD (open symbols) or DM (filled symbols) methods, with mixtures of the labeled K107C (circles), K133C (triangles) or K226C (squares) mutants with different proportions of the unlabeled wild type protein. The anisotropy values modified as $r_T (1-f_L E_{SQ})$ are plotted versus the molar fraction of labeled protein (f_L). Data are the means of 5 determinations. Standard deviations are in the order of the symbol size (≤ 0.005 anisotropy units). The values for the anisotropies in either the absence (r1 or rLU) or in the presence (r2 or rLL) of homo-FRET, calculated by fitting equation 18 to the data, are given in the figure insert.

Figure 5. Cholesterol efflux from RAW macrophages evoked by D-HDL. RAW 264.7 macrophages charged with ^{14}C-cholesterol were treated with different concentrations of D-HDL prepared by the CD (open symbols) or DM (filled symbols) methods with serum (circles) or recombinant (squares) apoAI. After 12 h, radioactivity was counted in media and cells. Efflux is expressed as the percentage of the radioactivity found in media relative to the total radioactivity in cells plus media. Data are the mean (and standard deviations) of five determinations.

Figure 1

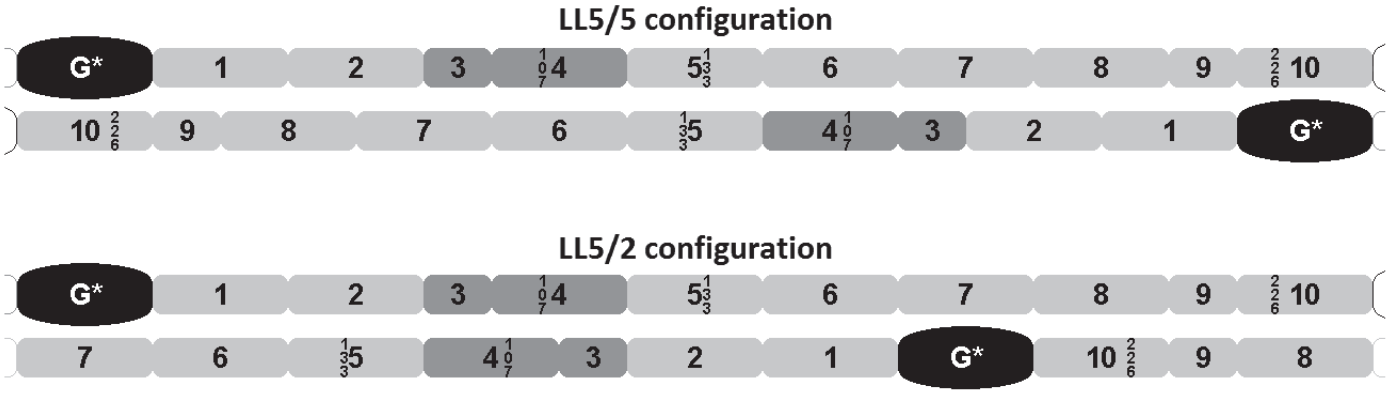
LL5/5 configuration
G*
1
2
3
4
5
6
7
8
9
10
10
9
8
7
6
5
4
3
2
1
G*
LL5/2 configuration
G*
1
2
3
4
5
6
7
8
9
10
7
6
5
4
3
2
1
G*
10
9
8

Figure 2

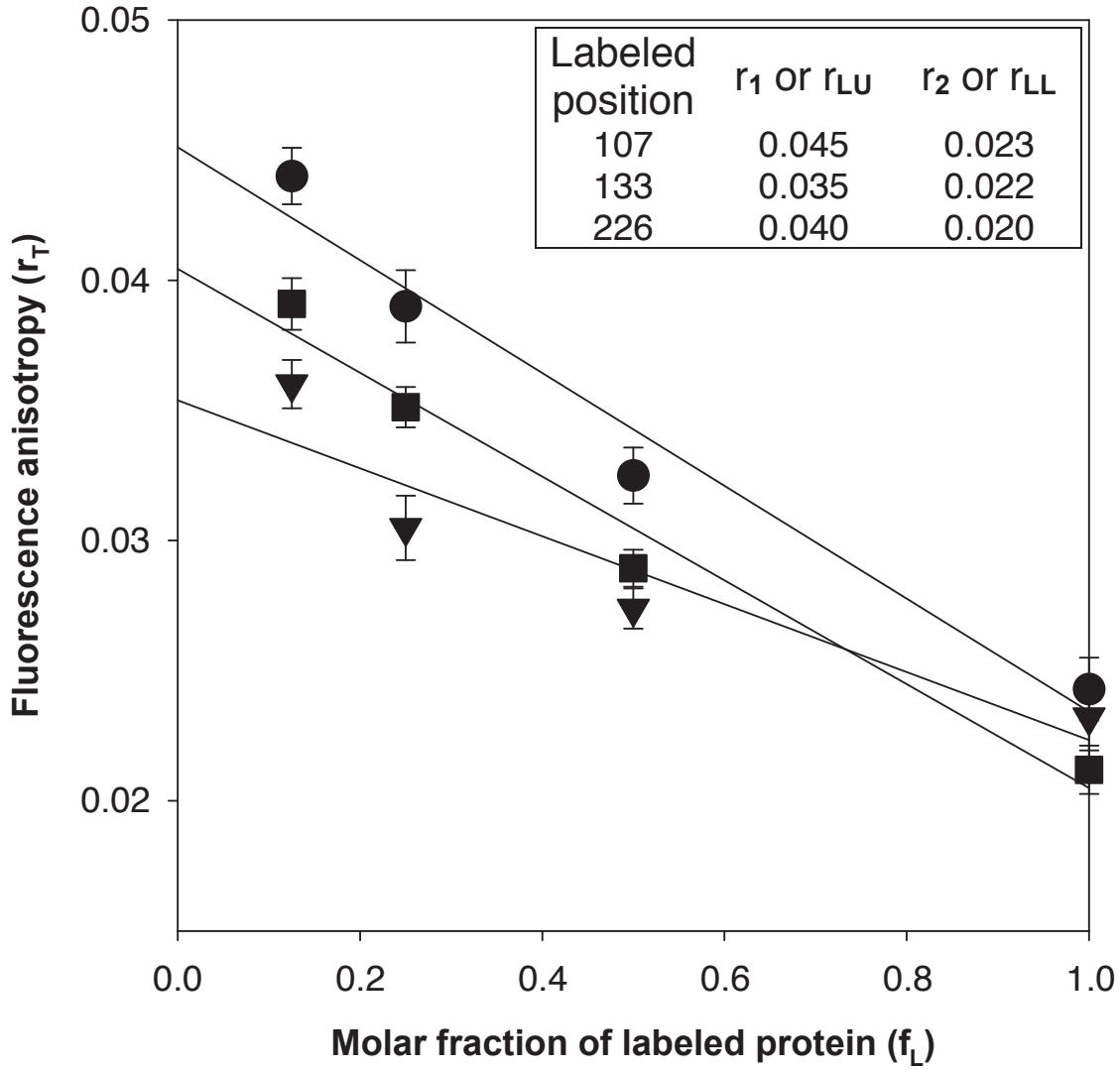
0.05
0.04
0.03
0.02
0.0
0.2
0.4
0.6
0.8
1.0
Fluorescence anisotropy (r_T)
Molar fraction of labeled protein (f_L)
Labeled position
r_1 or r_{LU}
r_2 or r_{LL}
107 0.045 0.023
133 0.035 0.022
226 0.040 0.020

Figure 3

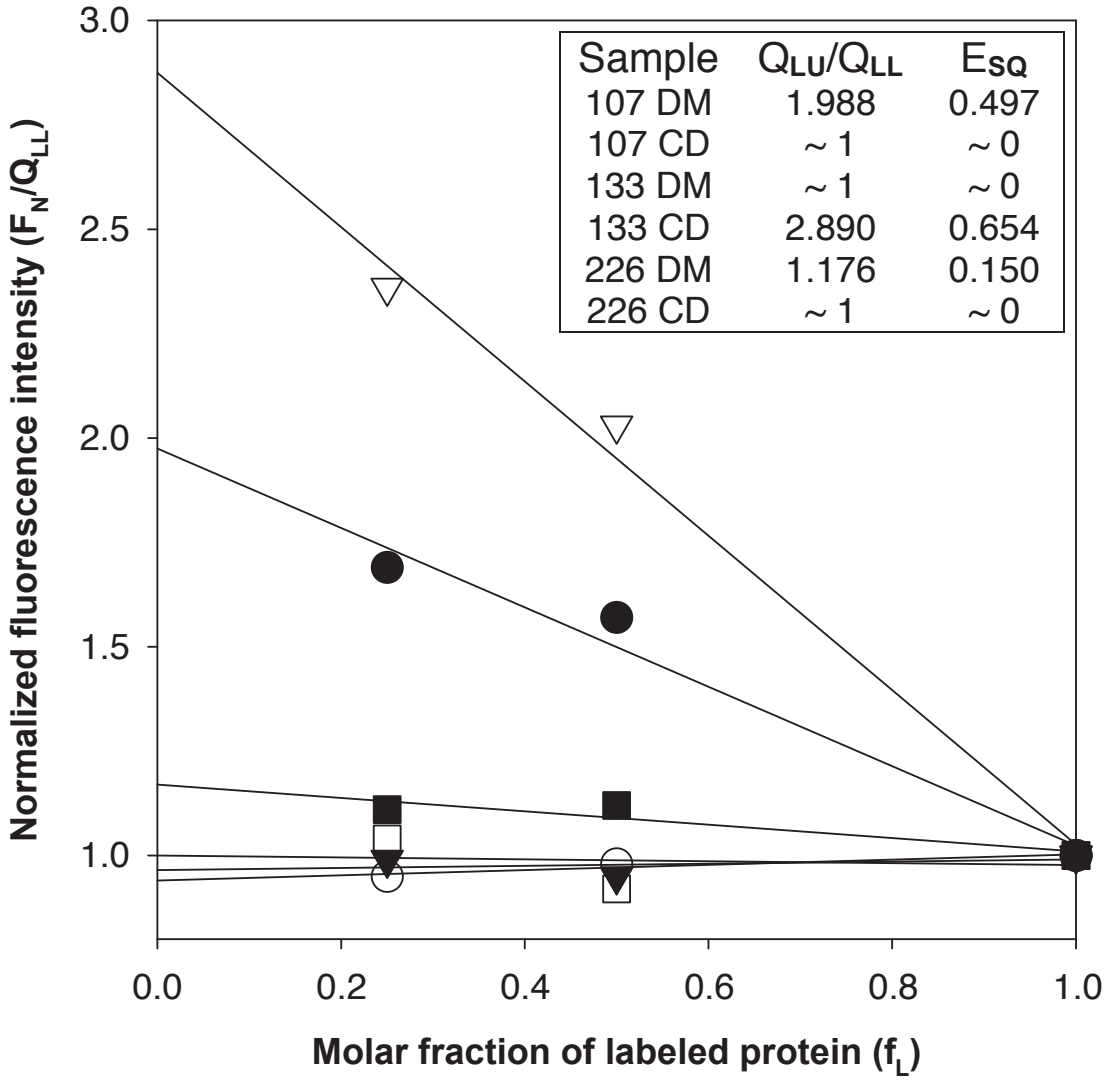
Sample
Q_{LU}/Q_{LL}
E_{SQ}
107 DM
1.988
0.497
107 CD
~ 1
~ 0
133 DM
~ 1
~ 0
133 CD
2.890
0.654
226 DM
1.176
0.150
226 CD
~ 1
~ 0
Normalized fluorescence intensity (F_N/Q_{LL})
3.0
2.5
2.0
1.5
1.0
0.0
0.2
0.4
0.6
0.8
1.0
Molar fraction of labeled protein (f_L)

Figure 4

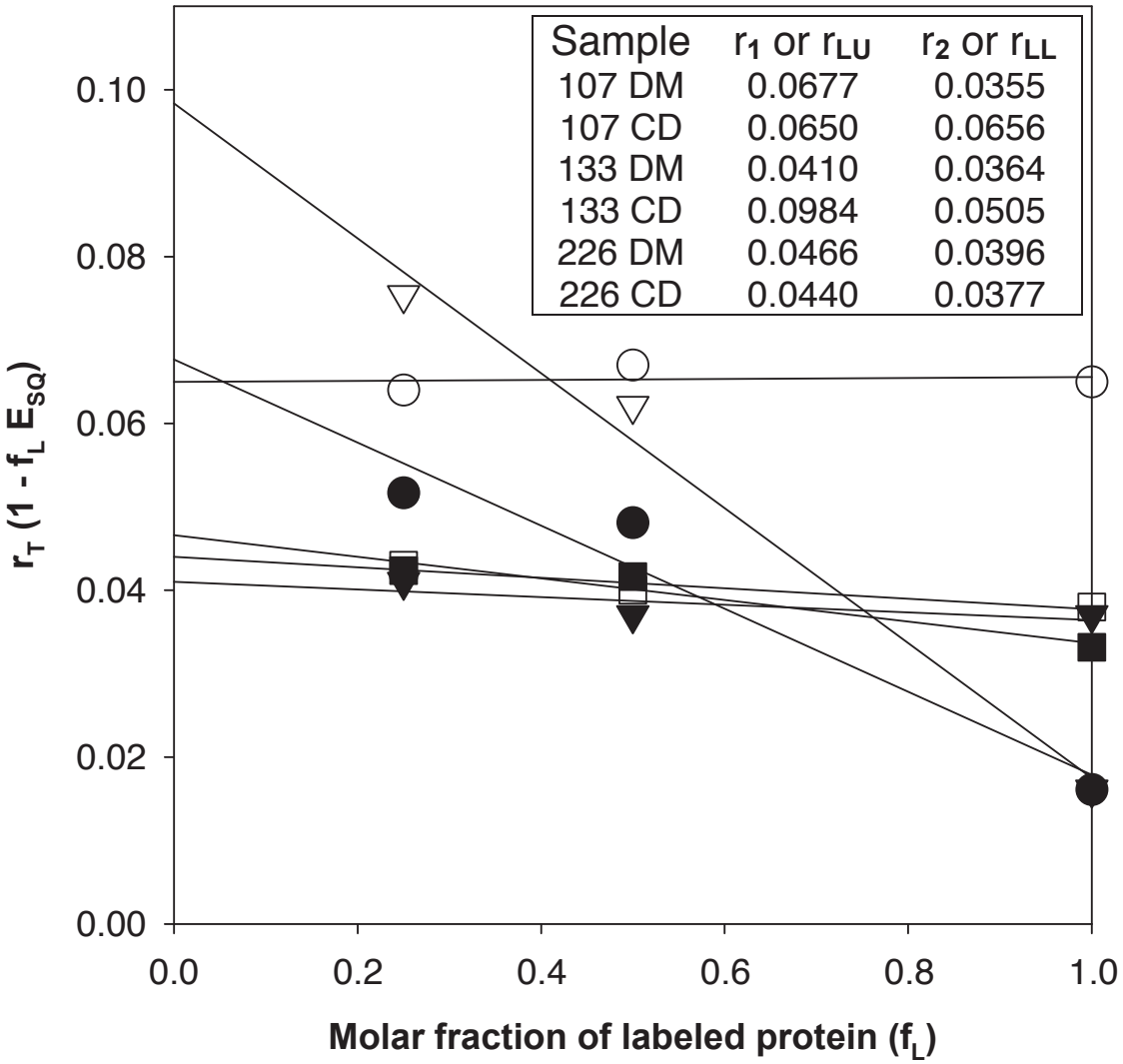
Sample | r1 or rLU | r2 or rLL
107 DM | 0.0677 | 0.0355
107 CD | 0.0650 | 0.0656
133 DM | 0.0410 | 0.0364
133 CD | 0.0984 | 0.0505
226 DM | 0.0466 | 0.0396
226 CD | 0.0440 | 0.0377
0.10
0.08
0.06
0.04
0.02
0.00
0.0
0.2
0.4
0.6
0.8
1.0
rT (1 - fL ESQ)
Molar fraction of labeled protein (fL)

Figure 5

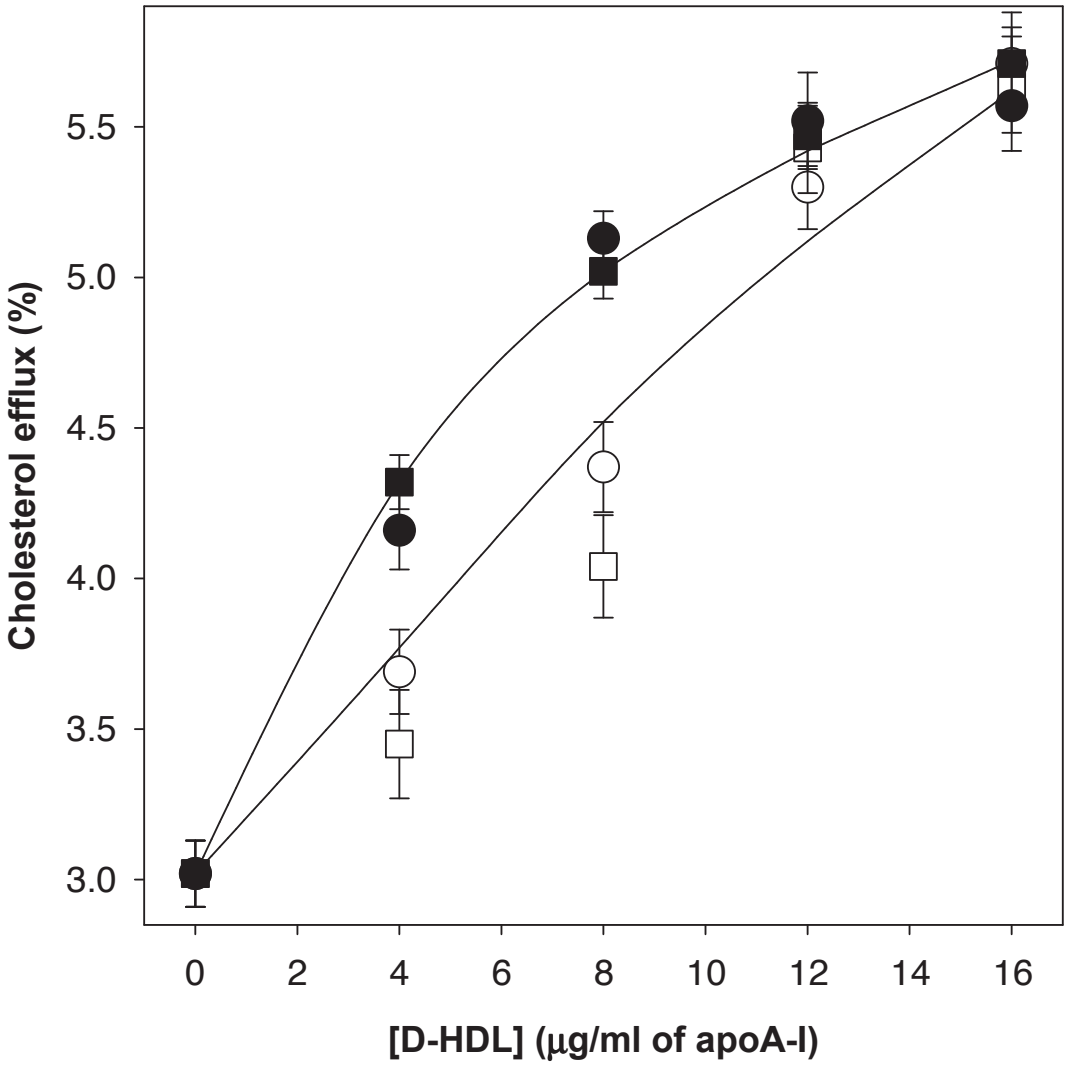
Cholesterol efflux (%)
5.5
5.0
4.5
4.0
3.5
3.0
0
2
4
6
8
10
12
14
16
[D-HDL] (µg/ml of apoA-I)

SUPPLEMENTAL DATA

Table S-I. Primers used for constructing K107C, K133C and K226C mutants of apoA-I

Mutant	Sequence (5'→3')	
K107C	CGACTTCCAGAAG**AAG**TGGCAGGAGG	(Original sequence)
	CGACTTCCAGAAG**TGT**TGGCAGGAGG	(Forward primer)
	CCTCCTGCCA**ACA**CTTCTGGAAGTCG	(Reverse primer)
K133C	GCGCGCGCCAG**AAG**CTGCACGAGCTG	(Original sequence)
	GCGCGCGCCAG**TGT**CTGCACGAGCTG	(Forward primer)
	CAGCTCGTGCAG**ACA**CTGGCGCGCGC	(Reverse primer)
K226C	GCCCGTGCTGGAGAGCTTC**AAG**GTCAGCTTCCTG	(Original sequence)
	GCCCGTGCTGGAGAGCTTC**TGT**GTCAGCTTCCTG	(Forward primer)
	CAGGAAGCTGAC**ACA**GAAGCTCTCCAGCACGGGC	(Reverse primer)

Table S-II. Stability and spectral properties of K107C, K133C and K226C mutants in comparison with the recombinant wild type apoA-I.

	Wild type[a]	K107C	K133C	K226C
λ_{max} (nm)[b]	339 ± 2	339 ± 2	340 ± 2	339 ± 2
ΔG^{O} (Kcal/mol)[c]	2.90 ± 0.2	2.89 ± 0.2	2.91 ± 0.2	2.88 ± 0.2
m[d]	1693 ± 100	1710 ± 100	1715 ± 100	1708 ± 100
$_{1/2}$[GdnHCl] (M)[e]	1.50 ± 0.04	1.52 ± 0.02	1.54 ± 0.04	1.53 ± 0.04
K (M^{-1})[f]	6.25 ± 1.10	6.26 ± 1.10	6.23 ± 1.10	6.30 ± 1.10
fa[g]	0.79 ± 0.01	0.79 ± 0.01	0.80 ± 0.01	0.79 ± 0.01
E[h]	0.28 ± 0.02	0.27 ± 0.02	0.28 ± 0.01	0.28 ± 0.01

[a] Data for wild type protein are from reference (34)
[b] Wavelength of maximum fluorescence of Trp residues under native conditions
[c,d,e] Are the free energy change of unfolding, the relative exposure of the hydrophobic surface area and GdnHCl concentration of half denaturation respectively, calculated from equilibrium unfolding curves as described previously (34)
[f,g] Are the Stern–Volmer constant and fluorophore fraction accessible to acrylamide quenching, respectively.
[h] Efficiency of energy transfer from tryptophan (as donor) to bis-ANS (as acceptor).

Table S-III. Properties of fluorescent probes and probe pairs used in homo- end hetero-FRET measurements.

Donor	Acceptor	ε_{Amax} ($M^{-1}cm^{-1}$)	Q_D	$J_{(\lambda)}$	R_O (nm)	Sensitivity range (nm)
Homo-FRET						
Alexa-350		**$1.9\ 10^4$**	**0.55**	**$6.6\ 10^{11}$**	**1.3**	**0.8 - 2.2**
Alexa-488		$7.2\ 10^4$	0.92	$7.3\ 10^{14}$	4.7	2.8 - 8.0
Alexa-488-Pr		**$7.2\ 10^4$**	**0.92**	**$1.2\ 10^{15}$**	**5.1**	**3.1 - 8.7**
Hetero-FRET						
A-350	A-488	$7.2\ 10^4$	0.55	$1.0\ 10^{15}$	4.5	2.7 - 7.6
A-350	**A-488-Pr**	**$7.2\ 10^4$**	**0.55**	**$9.3\ 10^{14}$**	**4.5**	**2.7 - 7.6**
A-350	**A-647**	**$2.6\ 10^5$**	**0.55**	**$7.6\ 10^{13}$**	**2.9**	**1.7 - 4.9**

The values for the acceptor extinction coefficient at the wavelength of the absorption maximum (ε_{Amax}) and quantum yield (Q_D) are those given in the probe instruction manuals provided by Molecular Probes. The overlap integrals ($J_{(\lambda)}$) and Föster distances (R_O) were calculated from equations 2 and 3 given in Experimental Procedures. Sensitivity ranges correspond to the limits between 0.6 and 1.7 R_O (or between 5 and 95% of FRET efficiency) where distances can be measured with acceptable precision. In the case of Alexa-488 (which presents a considerable blue shift in the absorption and emission spectra when it is covalently bound to the protein), data are given for the free and protein-bound (Alexa-488-Pr) probes.

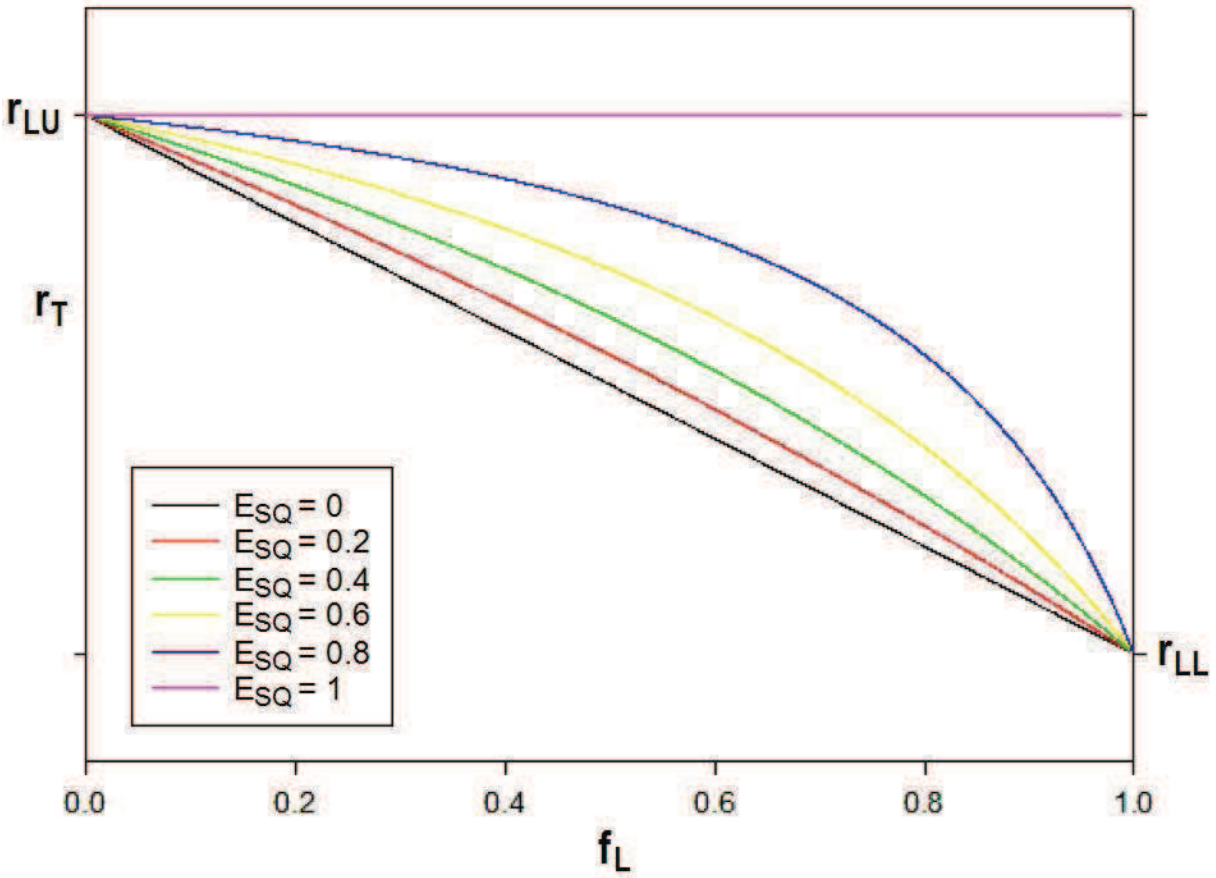

Figure S-1. Self-quenching influence on homo-FRET measurements. Theoretical plots of the total anisotropy (r_T) as a function of the molar fraction of labeled protein (f_L) for different self-quenching efficiencies (E_{SQ}) according to equation 17. Note that self-quenching influence can be ignored for $E_{SQ} \leq 0.2$.

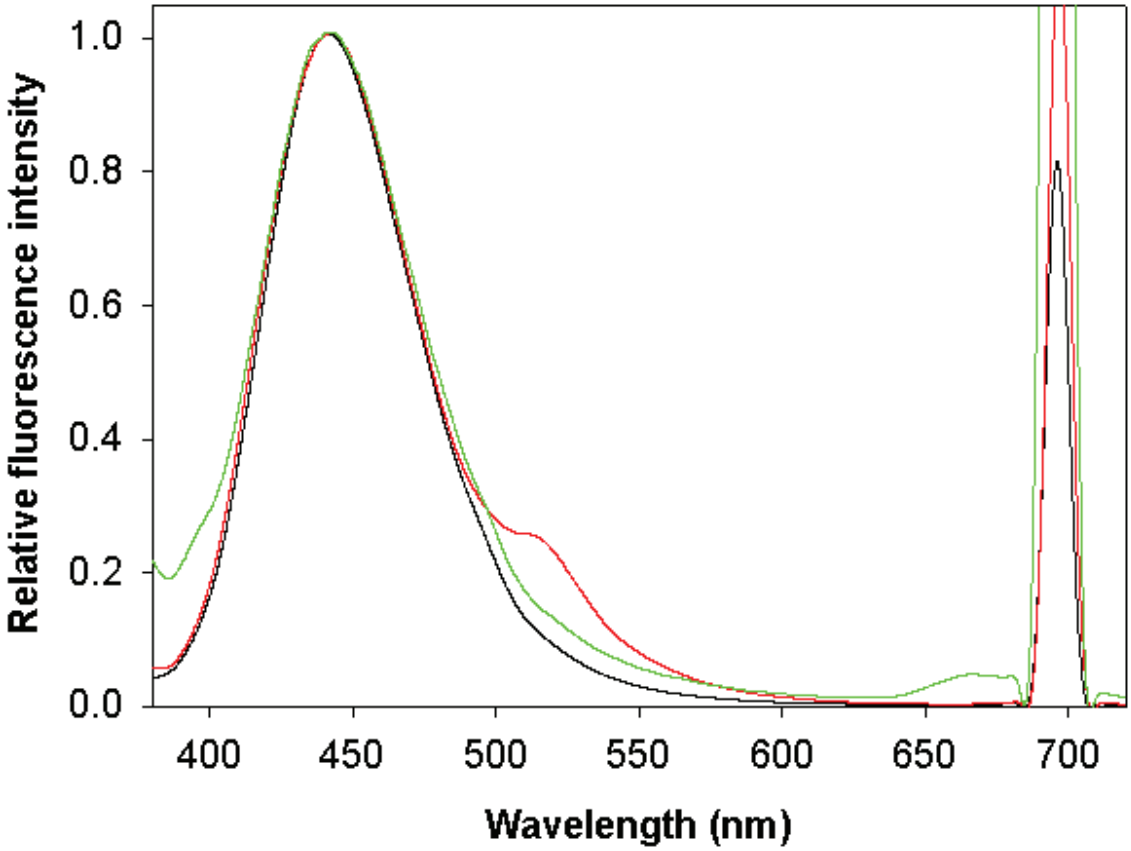

Figure S-2. Hetero-FRET measurements with Alexa-350 as donor and Alexa-488 or Alexa-647 as acceptors. Emission spectra of D-HDL prepared by DM with the mutant labeled with Alexa-350 in position 226 mixed in equimolar proportion with: a) the unlabeled wild type protein (black curve), b) the mutant 226 labeled with Alexa-488 (red curve), or c) the mutant 226 labeled with Alexa-647 (green curve). Note the increased acceptor emission in the region of 520 nm when the acceptor is Alexa-488 or in the region of 680 nm when the acceptor is Alexa-647 (visible in spite of the 2nd. order scattering peak at 700 nm). A wavelength of 350 nm was used for excitation.